energies

MDPI

Article

Effects of Temperature and Chemical Speciation of Mineral Elements on PM10 Formation during Zhundong Coal Combustion

Qiaoqun Sun [1], Zhiqi Zhao [2], Shizhang Wang [2], Yu Zhang [2,*], Yaodong Da [3], Heming Dong [2], Jiwang Wen [3], Qian Du [2] and Jianmin Gao [2]

[1] School of Aerospace and Construction Engineering, Harbin Engineering University, Harbin 150001, China
[2] School of Energy Science and Engineering, Harbin Institute of Technology, Harbin 150001, China
[3] China Institute of Special Equipment Inspection, Beijing 100029, China
* Correspondence: zhang.y@hit.edu.cn

Abstract: Particulate matter (PM) pollution from coal combustion is a leading contributor to the influence of atmospheric visibility, photochemical smog, and even global climate. A drop tube furnace was employed to explore the effects of temperature and chemical speciation of mineral elements on PM formation during the combustion of Zhundong coal. Chemical fractionation analysis (CFA), X-ray fluorescence (XRF), and inductively coupled plasma-atomic emission spectrometry (ICP-AES) were used to investigate the chemical and physical characteristics of the solid samples. It can be indicated that the combustion of similarly sized coal particles yielded more PM10 when the combustion temperature was increased from 1000 to 1400 °C. Zhundong coal is fractionated with deionized water, ammonium acetate, and hydrochloric acid, and pulverized coal, after fractionation, is burned to study the influence of mineral elements with different occurrence forms, such as water-soluble mineral elements, exchangeable ion elements, hydrochloric acid soluble elements and acid-insoluble elements, on the formation of particles. The results show that water-soluble salts play an important role in forming ultrafine particles (PM0.2); Fe, Ca, and other elements in organic form are distributed in flue gas through evaporation during pulverized coal combustion. When the flue gas temperature decreases, PM1 is formed through homogeneous nucleation and heterogeneous condensation, resulting in the distribution of these two elements on PM1. Different fractionation methods do not significantly affect the distribution of Si and Al in the PM1–10 combustion process.

Keywords: particulate matter (PM); Zhundong coal; PM10; PM1; PM0.2

Citation: Sun, Q.; Zhao, Z.; Wang, S.; Zhang, Y.; Da, Y.; Dong, H.; Wen, J.; Du, Q.; Gao, J. Effects of Temperature and Chemical Speciation of Mineral Elements on PM10 Formation during Zhundong Coal Combustion. *Energies* **2023**, *16*, 310. https://doi.org/10.3390/en16010310

Academic Editor: Fernando Rubiera González

Received: 27 October 2022
Revised: 30 November 2022
Accepted: 1 December 2022
Published: 27 December 2022

1. Introduction

Airborne particulate matter (PM) has become a major air pollutant in urban China in recent years. It is a leading factor contributing to decreased atmospheric visibility, global climate change, and photochemical smog [1–3]. PM is a complex mixture of organic substances and inorganic matter [4,5], including solid particles and liquid droplets. PM10 with an aerodynamic diameter of fewer than 10 μm can be breathed in through the nose/mouth and enter the human respiratory tract. Within the PM10 classification, PM can be further classified into submicron particulate matter (PM1) and ultra-micro particulate matter (PM1–10).

China accounts for 23% of the world's energy consumption, and, in the short term, at least, coal will remain the dominant source of Chinese energy [6]. Large reserves of Zhundong (ZD) coal exist in China [7], but the raw coal contains levels of alkali metals and alkaline earth metals (AAEMs) that are far higher than those found in other coals [8,9]. Combusting coals with significant AAEM species can lead to multi-particle formation during combustion, which can result in slagging and fouling problems and limit the utilization of ZD coal in large-scale applications [10,11].

Several variables impact the composition and formation characteristics of PM10. For example, increasing the combustion temperature would increase the number of PM10 produced [12–14]. Changing the mineral content in raw coal can influence how the mineral components react with each other during combustion, producing ash with different compositions that [15], in turn, influence the ash melting point. An increase in the ash melting point increases the formation of PM10, while an increase in the S content in the raw coal increases the production of PM1 [16]. A high silicate content in coal ash increases the melting temperature, while a high content of oxides and sulfate tends to lower its fusion temperature [17]. In addition, coal's mineral content and the division between organic and inorganic fractions can significantly influence PM formation [18,19]. Among others, Na, K, Ca, Al, and Fe can promote lower-temperature melting and polymerization of fine particles, forming larger particles [11,20,21]. PM1 mainly comprises alkali metal oxides, refractory oxides, and sulfides [16]. High-Na/K coals burn at 900–1100 °C, with the sulfate core forming the main component of PM1. At 1300 °C, Na and K elements are precipitated as hydroxides and easily combine with aluminate in coal to form larger particles (PM10+) [22]. The occurrence of Ca and Mg elements in low-rank coal is the primary determinant of their precipitation behavior [23,24]. Al is mainly present in the form of aluminosilicate, with less precipitation.

During combustion, various forms of different mineral elements precipitate at different stages, impacting PM formation with various sizes. Indeed, relatively few studies have been carried out addressing the impact of mineral matter composition on PM formation and composition characteristics. The work aims to provide helpful information that will aid the control of PM pollution from coal combustion.

2. Material and Methods

2.1. Sample Preparation

As shown in Figure 1, the drop tube furnace (DTF) was used for experiments with Chinese ZD coal (90–125 μm). The experiment was carried out in the air at 1000–1400 °C. The furnace was composed of a corundum tube of 80 mm diameter and 2000 mm length. The pulverized coal sample was pneumatically conveyed into the furnace chamber at a constant rate of 1.0 g/min with the primary air. The primary air flow is 1 L/min, and the secondary airflow is 9 L/min. A secondary air was mixed at the burner to ensure the burn-out rate in the furnace [25]. Fly ash was collected at the bottom of the reactor. The proximate and ultimate analyses of ZD coal are listed in Table 1. The compositional analysis of raw ZD coal ash is listed in Table 2.

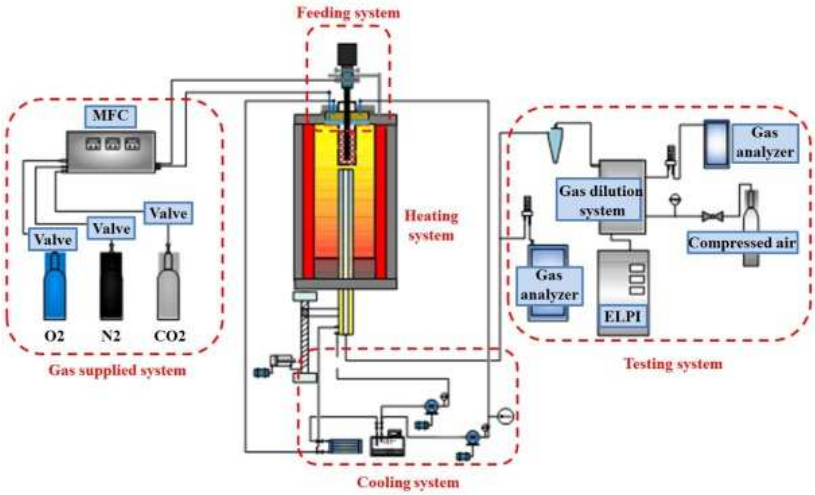

Figure 1. Schematic diagram of the experimental furnace.

Table 1. Proximate and ultimate analysis of ZD coal.

Proximate Analysis (wt.%, ad. = Air Dry Basis)				Ultimate Analysis (wt.%, ad. = Air Dry Basis)				
M(Moisture)	**A(Ash)**	**V(Volatile)**	**FC(Fixed Carbon)**	**C**	**H**	**Odiff.**	**N**	**S**
9.63	5.5	40.3	44.57	61.4	4.41	17.69	0.89	0.48

Note: Heating value = 18.5 MJ/kg. diff. = by difference.

Table 2. Compositional analysis of ZD coal ash.

Ash Compositions (wt. %)										
SiO_2	**Al_2O_3**	**Fe_2O_3**	**CaO**	**MgO**	**TiO_2**	**SO_3**	**MnO_2**	**K_2O**	**P_2O_5**	**Na_2O**
30.56	29.85	10.56	8.64	4.42	0.22	7.66	0.31	0.6	0.12	6.02

2.2. Chemical Fractionation Analysis

The chemical speciation of mineral elements in raw ZD coal was assessed by chemical fractionation analysis (CFA) [26–29]. Samples were dried overnight at 105 °C, and then each sample was successively extracted with deionized water (H_2O), 1.0 mol/L ammonium acetate (NH_4Ac), and 1.0 mol/L hydrochloric acid (HCl). In the first extraction, H_2O-soluble compounds, such as K and Na salts, would be dissolved [30]. Organically bound ion-exchangeable elements were removed by the NH_4Ac solution [31]. Finally, acid-soluble compounds, such as carbonates and sulfates, were extracted using an HCl solution. After each extraction, the solid residue was washed with deionized water until the pH of the leachate was constant. According to the procedures carried out during the CFA process, the samples were named raw coal, H_2O-coal, NH_4Ac-coal, and HCl-coal, respectively. These samples were then introduced to the DTF in the same way as the raw coal at 1200 °C.

2.3. Sampling System

PM samples were simultaneously sampled from the collected ash and classified for analysis. In order to study the morphology and composition, polycarbonate film was used for microscopic analysis [32]. A Teflon filter membrane was used during inorganic content analysis using ICP-AES and XRF.

An electrical low-pressure impactor (ELPI) (97 2E, NO.24423, Dekati LTD, Kangasala, Finland) was used to measure the ash particle size distribution. X-ray fluorescence (XRF, PW4400) further developed the compositional analysis. Major (content more than 1000 g/g) and minor (in 100~1000 g/g) ash components were then qualitatively and semi-quantitatively analyzed with accurate detection of elements in the range 9F to 92U. A vacuum of less than 100 Pa (minimum 1 Pa) and a temperature of approximately 60–70 °C were used; these conditions were assumed not to denature the sample.

The mineral matter that was retained in the ash particles was digested by a microwave digestion system (Ethos 1, Milestone, Sorisole, Italy) [29]. Each digested residue was re-dissolved, transferred to a 25 mL volumetric flask, and made up to a set volume with deionized H_2O. The mineral elements were then quantified by an inductively coupled plasma atomic emission spectrometer (ICP-AES).

3. Results and Discussion

3.1. Impact of Temperature on PM10 Formation

As shown in Figure 2, the impact of Raw-coal's combustion temperature on the formation of variously sized PM can be seen. Figure 2a shows a similar distribution for all temperatures. The amount of PM10 formed increased as the combustion temperature increased. The peak at approximately 2 μm was mainly affected by the formation of PM1–10 particles. At higher temperatures, the internal temperature gradient of the char particles is steeper, and the particles endure a relatively higher level of thermal stress, rendering them easily broken [33,34]. Figure 2b initially shows a gradual increase in the amount of PM0.2, from 0.29 to 0.32 mg/g, as the temperature was increased from 1000 to 1200 °C, with a more significant increase to 0.37 mg/g at 1400 °C. This might be driven by increased evaporation

and condensation of mineral elements at higher temperatures [35]. The amount of PM0.2–1 produced is similar at 1000 and 1200 °C (0.30 and 0.31 mg/g, respectively), but it increases to 0.37 mg/g at 1400 °C. The amount of PM1 increases to 0.62 mg/g and 0.74 mg/g. A similar trend was observed for the different temperatures for particles in the PM10 and PM1 ranges. Results at 1000, 1200, and 1400 °C yielded 0.57, 0.61, and 0.71 mg/g for PM1–10 and 1.15, 1.23, and 1.46 mg/g for PM10, respectively. The precipitation and condensation of mineral elements were the primary mechanisms for forming PM1 [16,36,37]. The extent to which mineral elements volatilize is known to be positively correlated with the amount of PM1 [38], and, in general, their vapor-phase concentration is high. At the same time, the associated particle enjoys a slight temperature gradient across it, a long aggregation time, and a relatively large size [39].

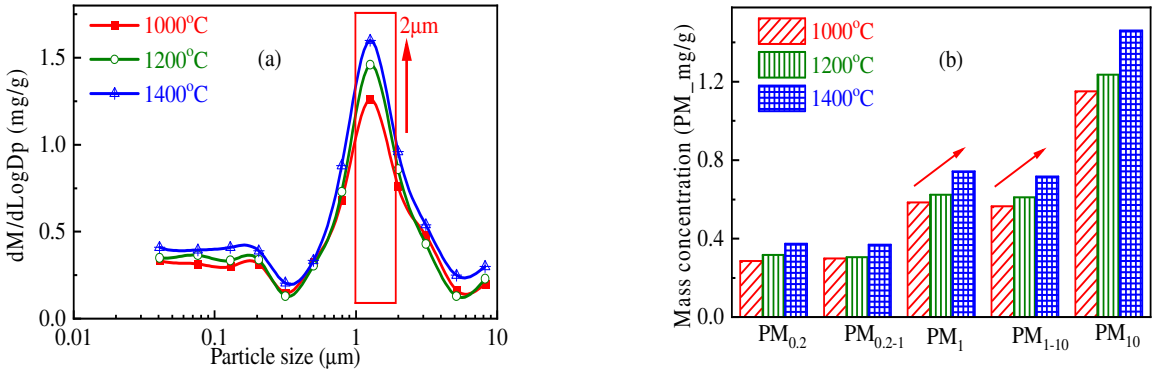

Figure 2. Continuous (**a**) and discrete (**b**) distribution of PM10 at different temperatures.

An analysis of the major mineral components in PM10 combusted at different temperatures is shown in Figure 3, while Figure 4 presents the bulk compositions of PM with various sizes. For PM0.2, an increase of the combustion temperature from 1000 to 1200 and then to 1400 °C increased the mass fraction of K and particularly Na, which increased from 9.0 to 12.5 and then to 20.6%. The change of element S is basically the same. Figure 4b shows that compared with the results for PM0.2, the PM0.2–1 fraction exhibited a significantly lower mass fraction of the volatile components but a much higher proportion of the non-volatile (Ca, Mg, and Fe) elements and Al-Si salts. (Under three temperature conditions, the proportion of volatile elements in PM0.2 is 26.28%, 29.40%, and 37.08%, respectively. The proportion of volatile elements in PM0.2–1 is 7.00%, 8.12%, and 12.66%, respectively). Because the mineral substances needed for particle nucleation come from two sources: the volatilization of minerals or their release during coal combustion [40]. This can be explained by considering that PM10 is more likely to be formed by homogeneous nucleation mechanisms and the condensation of volatile elements on the particle surface [41–44]. The main reason for the difference in mineral content in PM0.2 and PM0.2+ particles is that the formation mechanism of particles with different sizes is different. The content of volatile elements in PM0.2 is high. PM0.2 is mainly formed by steam condensation. The steam source is the decomposition of mineral elements in organic form in the coal powder pyrolysis stage, releasing mineral steam or the formation of inorganic minerals in the coke combustion stage. PM0.2+ is mainly generated in the coke combustion stage, mainly including volatile elements condensed on fine particles and particles rich in silicon and aluminum formed in the molten state, which accumulates to form irregular particles. As shown in Figure 4c, the content of volatile mineral elements in PM1–10 was less than that in the other samples. The fraction of volatile elements in the samples at 1200/1400 °C is very similar (6.2 and 6.9%, respectively), significantly greater than that observed at 1000 °C (1.7%). The most volatile elements reached the maximum value at 1400 °C, slightly increasing at 1200 °C.

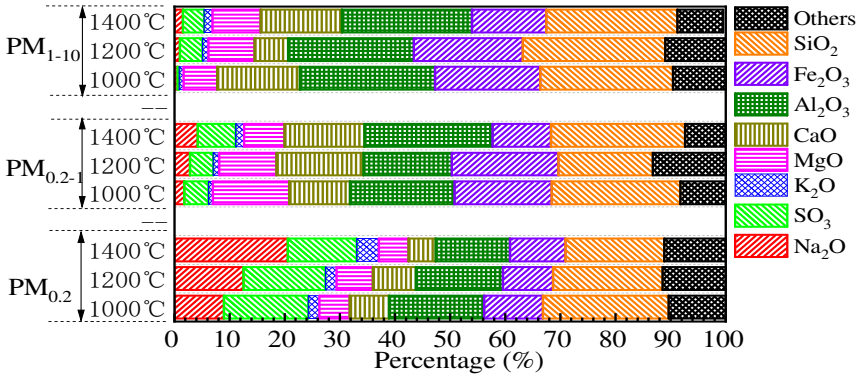

Figure 3. Composition of significant mineral components in PM10.

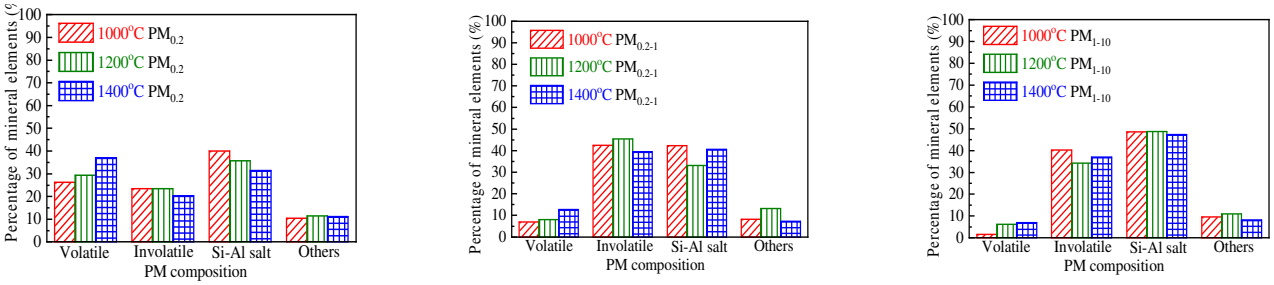

(**a**) PM0.2 (**b**) PM0.2–1 (**c**) PM1–10

Figure 4. Composition of various size fractions of coal ash generated at different combustion temperatures. Volatile denotes Na, K, and S; non-volatile denotes Mg, Ca, and Fe.

3.2. Effect of Chemical Speciation of Mineral Elements on PM10 Formation

3.2.1. Chemical Speciation of Mineral Elements

Table 3 shows the composition of significant elements for the four stages of CFA. At the same time, Figure 5 displays the main speciation of these inorganic elements depending on whether they are soluble in H_2O, NH_4Ac, or HCl or insoluble in all the above solvents. The highest compositions observed in the raw sample are for Al and Si, followed by Fe, Ca, and Na. Na is mainly found as an H_2O-soluble salt. Washing with H_2O removes 61.1% of the actual Na, though this process removes little Mg, Ca, Fe, or Al. Washing with NH_4Ac removes 32.1% of the Mg and 20.2% of the Ca remaining after the H_2O wash. Mg and Ca species that then dissolve in HCl but are insoluble in NH_4Ac mainly comprised carbonates [45–48], such as calcite ($CaCO_3$) and dolomite ($CaMg(CO_3)_2$). Washing with HCl dissolves 39.2% of Al with the insoluble fraction assumed to be aluminosilicates, such as kaolin. For Fe, 17.9% is NH_4Ac-soluble, 44.7% is HCl-soluble, and the remainder consists of insoluble salts. With most Fe compounds insoluble in H_2O, compounds soluble in HCl or NH_4Ac may include siderite ($FeCO_3$) [49], ankerite ($(FeCaMg)CO_3$), or Fe(OH). Fe compounds that are insoluble in HCl may have been pyrite (FeS_2).

Table 3. Content of mineral elements in CFA (mg/g).

Coal	K	Na	Ca	Mg	Fe	Al	Si	Ash
Raw-Coal	0.2	1.8	2.6	1.2	2.8	6.9	6.8	5.3
H_2O-Coal	0.1	0.7	2.4	1.1	2.5	6.4	6.0	4.6
NH_4Ac-Coal	0.1	0.6	1.9	0.8	2.3	5.8	5.3	3.9
HCl-Coal	0.1	0.1	0.2	0.1	1.0	3.1	2.0	1.2

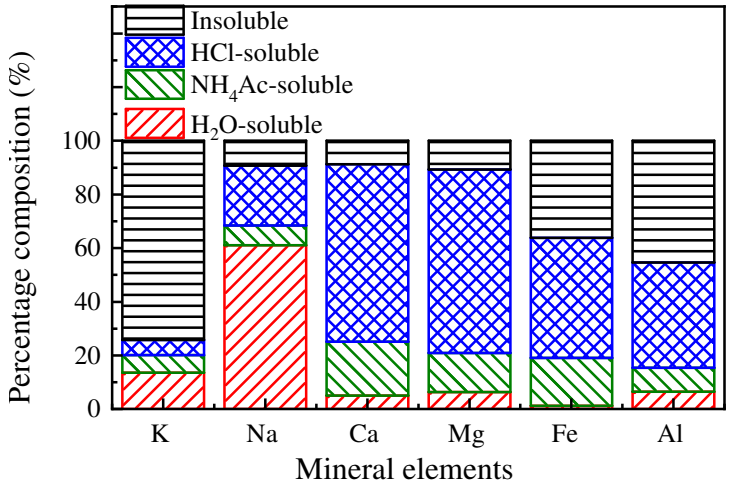

Figure 5. Fractionation of major elements.

3.2.2. Distribution of the Primary Mineral in PM10

CFA results showing the major mineral components for PM0.2, PM0.2–1, and PM1–10 are shown in Figure 6. The main components of PM0.2 were volatile elements such as S, Na, and K. The proportions of the insoluble elements—Mg, Ca, Fe, Al, and Si—were relatively small. The PM0.2 content of Na decreased significantly following H_2O-washing. At the same time, acid-washing caused an increase in the concentration of Si and Al elements as other mineral elements (such as Mg, Ca, and Fe) dissolved in HCl. The PM0.2–1 and PM1–10 fractions generated from the combustion of four different coal samples were very similar and mainly comprised refractory oxides (of Mg, Ca, and Fe) and Al and Si compounds. A bulk analysis of the composition of the three PM size groups is shown in Figure 7. These results suggest that the PM samples were mainly composed of Na_2O, MgO, CaO, SiO_2, Al_2O_3, Fe_2O_3, SO_3, and K_2O.

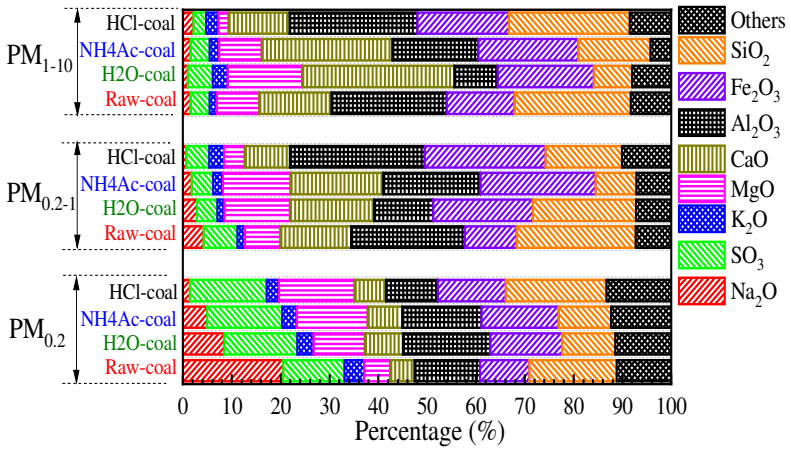

Figure 6. Major mineral in PM10 from CFA-treated coal samples.

3.2.3. Speciation of Mineral Elements in PM10

The impact of various treatments of the coal samples on the ash particle size distribution can be seen in Figure 8a. Notably, the acid-treated coal sample displayed no apparent peak in PM distribution, which was relatively uniform. Indeed, the ash content of the raw coal sample decreased from 5.3% to 1.2% after the acid-washing process. The PM distribution shows the two distinct peaks divided into three areas: ultrafine, intermediate, and coarse. The precipitation of mineral elements forms ultrafine particles. ZD coal has a high H_2O-soluble alkali content (especially Na), much of which was removed following H_2O washing. The number of ultrafine particles was constant, indicating that

the ultrafine particles play an important part in the combustion process of coal with the H_2O-soluble minerals.

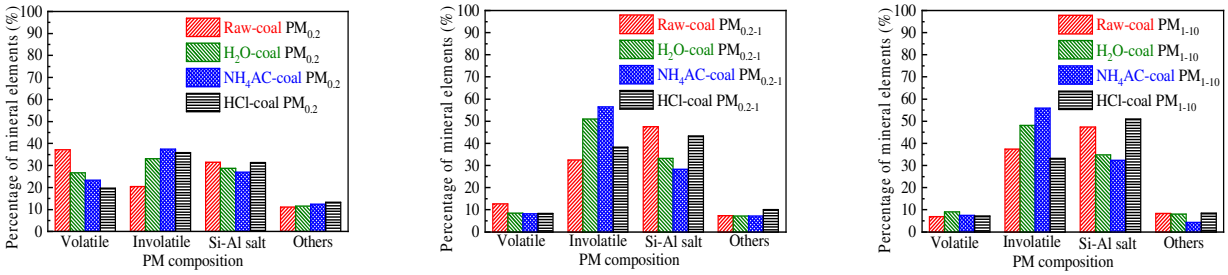

(**a**) PM0.2 (**b**) PM0.2–1 (**c**) PM1–10

Figure 7. Composition of various size fractions of coal ash generated from CFA-treated coal samples. Volatile denotes Na, K, and S; Non-volatile denotes Mg, Ca, and Fe.

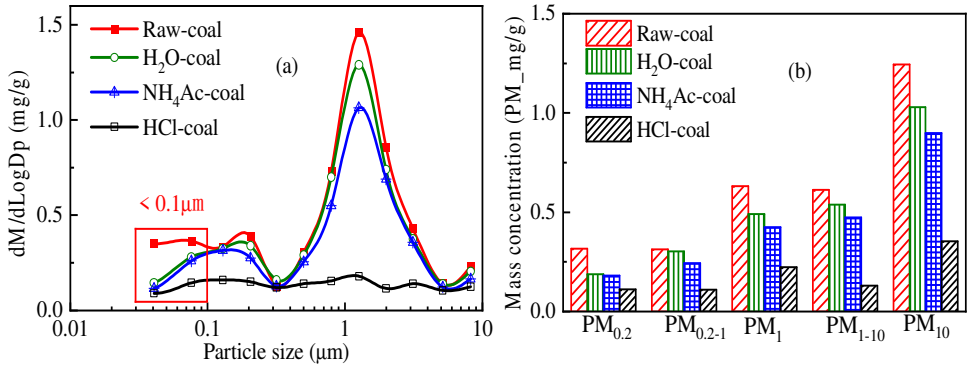

Figure 8. Continuous (**a**) and discrete (**b**) distribution of PM10 at different processing methods.

Na catalyzes the combustion process, accelerating the char burning rate and causing the particles to burn out more quickly. It decreases the accumulation time for melting ash and cannot adhere to the ash surface. Removing 61% of Na from the raw coal by H_2O-washing could decrease the reactivity of the char (compared with that of raw coal) during combustion. This decrease in reactivity may increase the accumulation and agglomeration time for the melting ash particles on the char surface, promoting the formation of larger particulates (>10 μm).

Figure 8 shows the particle size distribution for PM10 produced from the various coal samples. H_2O-washing caused the amount of PM0.2 to decrease from 0.32 to 0.19 mg/g, mainly because of the leaching of Na, which is key to the formation of particles via the evaporation–condensation mechanism in the PM0.2 range. Fine particulates mainly develop via two pathways: vapor condensation reactions at an inorganic surface of a nucleation point or the collision and coagulation of two existing fine particles [49]. The amount of PM0.2–1 generated from the combustion of raw coal, H_2O-coal, and NH_4Ac-coal was 0.31, 0.30, and 0.24 mg/g, respectively. From these results, it is possible to conclude that the role of H_2O-soluble mineral elements in the PM0.2–1 generation process is non-obvious and that the existence of the mineral elements in the H_2O-coal and raw coal (such as Ca, Fe, and Mg) suggests that organic minerals also impacted the formation of PM0.2–1. The fraction of ash produced as PM1–10 for the raw coal, H_2O-coal, NH_4Ac-coal, and HCl-coal samples was 0.61, 0.53, 0.47, and 0.13 mg/g, respectively, suggesting that the HCl-soluble minerals were essential in PM1–10 formations. These minerals may include carbonates, siderite, ankerite (Fe, Ca, Mg)O_3, or $Fe(OH)_2$. For the PM10 fraction, the raw coal produced 1.24 mg/g, which included 0.32 (25%), 0.31 (25%), and 0.61 (50%) mg/g of, respectively, PM0.2, PM0.2–1, and PM1–10. The fractional amounts of PM10 generated by the combustion of H_2O-coal, NH_4Ac-coal, and HCl-coal were all lower than that of raw coal (at 1.03, 0.90, and 0.35 mg/g, respectively). This analysis suggests that H_2O-soluble

mineral elements mainly affected the formation of PM0.2; organically bound elements impacted the amount of PM0.2–1 generated and washing with HCl significantly decreased the amount of PM1–10 produced by coal combustion.

4. Conclusions

(1) When Zhundong pulverized coal with the same combustion atmosphere and particle size burns, the total amount of PM10 generated at high combustion temperature is generally more. At 1000 °C, 1200 °C and 1400 °C, the amount of PM10 generated by the unit mass of Zhundong pulverized coal is 1.15 mg/g, 1.23 mg/g and 1.46 mg/g, respectively. The reason may be that with the increase in combustion temperature, the steam concentration of mineral elements in coal during combustion is increased. When the temperature decreases, more mineral steam will condense on the surface of particles.

(2) The mineral elements in raw coal are divided into water-soluble mineral elements, organically bound mineral elements, acid-soluble mineral elements and acid-insoluble mineral elements by chemical fractionation. Water-soluble salts play an important role in the formation of ultrafine particles (PM0.2). The organic Fe and Ca elements do not react with the aluminosilicate in the pulverized coal during the combustion of pulverized coal but evaporate into steam and distribute in the flue gas. When the flue gas temperature decreases, they condense and form on PM1, resulting in these two elements on PM1; Mg, Ca, and Fe react with aluminosilicate to form molten particles, which makes particles PM1–10 contain these three elements. Different fractionation methods will not greatly affect Si and Al in the PM1–10 combustion process.

Author Contributions: Conceptualization, Y.Z.; Software, J.W.; Resources, Y.D., H.D., Q.D. and J.G.; Data curation, Z.Z.; Writing—original draft, Q.S.; Writing—review & editing, S.W. All authors have read and agreed to the published version of the manuscript.

Funding: This work is supported by the National Natural Science Foundation of China (52006047), Heilongjiang Provincial Natural Science Foundation (LH2022E065) and Foundation of State Key Laboratory of High-Efficiency Utilization of Coal and Green Chemical Engineering (2021-K45).

Data Availability Statement: Date openly available in a public repository.

Conflicts of Interest: No conflict of interest.

References

1. Yao, Q.; Li, S.Q.; Xu, H.W.; Zhuo, J.K.; Song, Q. Studies on formation and control of combustion particulate matter in China: A review. *Energy* **2009**, *34*, 1296–1309. [CrossRef]
2. Chung, W.S.; Chen, Q.; Osammor, O.; Nolan, A.; Zhang, X.H.; Sharifi, V.N.; Swithenbank, J. Characterisation of particulate matter on the receptor level in a city environment. *Environ. Monit. Assess.* **2012**, *184*, 1471–1486. [CrossRef] [PubMed]
3. Fiore, A.M.; Naik, V.; Leibensperger, E.M. Air Quality and Climate Connections. *J. Air Waste Manag. Assoc.* **2015**, *65*, 645–685. [CrossRef] [PubMed]
4. Zhao, T.; Yan, Y.; Zhou, B.; Zhong, X.; Hu, X.; Zhang, L.; Huo, P.; Xiao, K.; Zhang, Y.; Zhang, Y. Insights into reactive oxygen species formation induced by water-soluble organic compounds and transition metals using spectroscopic method. *J. Environ. Sci.* **2023**, *124*, 835–845. [CrossRef] [PubMed]
5. Feng, D.D.; Guo, D.W.; Zhang, Y.; Sun, S.Z.; Zhao, Y.J.; Shang, Q.; Sun, H.L.; Wu, J.Q.; Tan, H.P. Functionalized construction of biochar with hierarchical pore structures and surface O-/N-containing groups for phenol adsorption. *Chem. Eng. J.* **2021**, *410*, 127707. [CrossRef]
6. Li, L.; Karatzos, S.; Saddler, J. The potential of forest-derived bioenergy to contribute to China's future energy and transportation fuel requirements. *For. Chron.* **2012**, *88*, 547–552. [CrossRef]
7. Zhang, X.-P.; Zhang, C.; Tan, P.; Li, X.; Fang, Q.-Y.; Chen, G. Effects of hydrothermal upgrading on the physicochemical structure and gasification characteristics of Zhundong coal. *Fuel Processing Technol.* **2018**, *172*, 200–208. [CrossRef]
8. Dai, S.; Ren, D.; Chou, C.L.; Finkelman, R.B.; Seredin, V.V.; Zhou, Y. Geochemistry of trace elements in Chinese coals: A review of abundances, genetic types, impacts on human health, and industrial utilization. *Int. J. Coal Geol.* **2011**, *94*, 3–21. [CrossRef]
9. Zhou, X.; Huang, D.; Guo, J.; Ning, H. Hydrogenation properties of Mg17Al12 doped with alkaline-earth metal (Be, Ca, Sr and Ba). *J. Alloys Compd.* **2019**, *774*, 865–872. [CrossRef]

10. Li, G.Y.; Wang, C.A.; Yan, Y.; Jin, X.; Liu, Y.H.; Che, D.F. Release and transformation of sodium during combustion of Zhundong coals. *J. Energy Inst.* **2016**, *89*, 48–56. [CrossRef]
11. Feng, D.D.; Shang, Q.; Dong, H.M.; Zhang, Y.; Wang, Z.L.; Li, D.; Xie, M.; Wei, Q.Y.; Zhao, Y.J.; Sun, S.Z. Catalytic mechanism of Na on coal pyrolysis-derived carbon black formation: Experiment and DFT simulation. *Fuel Process. Technol.* **2021**, *224*, 107011. [CrossRef]
12. Linak, W.P.; Miller, C.A.; Seames, W.S.; Wendt, J.O.L.; Ishinomori, T.; Endo, Y.; Miyamae, S. On trimodal particle size distributions in fly ash from pulverized-coal combustion. *Proc. Combust. Inst.* **2002**, *29*, 441–447. [CrossRef]
13. Jia, Y.; Lighty, J.A.S. Ash Particulate Formation from Pulverized Coal under Oxy-Fuel Combustion Conditions. *Environ. Sci. Technol.* **2012**, *46*, 5214–5221. [CrossRef]
14. Zhu, S.; Zhang, M.; Li, Z.; Zhang, Y.; Yang, H.; Sun, J.; Lyu, J. Influence of combustion temperature and coal types on alumina crystal phase formation of high-alumina coal ash. *Proc. Combust. Inst.* **2019**, *37*, 2919–2926. [CrossRef]
15. Ke, X.; Li, D.; Zhang, M.; Jeon, C.-h.; Cai, R.; Cai, J.; Lyu, J.; Yang, H. Ash formation characteristics of two Indonesian coals and the change of ash properties with particle size. *Fuel Process. Technol.* **2019**, *186*, 73–80. [CrossRef]
16. Buhre, B.J.P.; Hinkley, J.T.; Gupta, R.P.; Nelson, P.F.; Wall, T.F. Fine ash formation during combustion of pulverised coal–coal property impacts. *Fuel* **2006**, *85*, 185–193. [CrossRef]
17. Vassilev, S.V.; Kitano, K.; Takeda, S.; Tsurue, T. Influence of mineral and chemical-composition of coal ashes on their fusibility. *Fuel Processing Technol.* **1995**, *45*, 27–51. [CrossRef]
18. Liu, X.; Xu, M.; Yao, H.; Yu, D.; Lv, D. Study on the effect of the occurrence of sodium elements in coal on the formation of submicron particles. *J. Eng. Therm. Phys.* **2009**, *30*, 1589–1592.
19. Su, X.B.; Ding, R.; Zhuang, X.G. Characteristics of Dust in Coal Mines in Central North China and Its Research Significance. *ACS Omega* **2020**, *5*, 9233–9250. [CrossRef]
20. Yu, D. *Modal Identification and Formation Mechanism of Fine Particle in Coal Combustion*; Huazhong University of Science and Technology: Huazhong, China, 2007.
21. Feng, D.D.; Guo, D.W.; Shang, Q.; Zhao, Y.J.; Zhang, L.Y.; Guo, X.; Cheng, J.; Chang, G.Z.; Guo, Q.J.; Sun, S.Z. Mechanism of biochar-gas-tar-soot formation during pyrolysis of different biomass feedstocks: Effect of inherent metal species. *Fuel* **2021**, *293*, 120409. [CrossRef]
22. Zhou, K. *Study on the Generation Characteristics and Furnace Control of Fine Particulate Matter in Coal Combustion*; Huazhong University of Science and Technology: Huazhong, China, 2011.
23. Quann, R.J.; Sarofim, A.F. Vaporization of refractory oxides during pulverized coal combustion. *Symp. Combust.* **1982**, *19*, 1429–1440. [CrossRef]
24. Sun, J.; Guo, Y.; Yang, Y.; Li, W.; Zhou, Y.; Zhang, J.; Liu, W.; Zhao, C. Mode investigation of CO2 sorption enhancement for titanium dioxide-decorated CaO-based pellets. *Fuel* **2019**, *256*, 116009. [CrossRef]
25. Zheng, W.; Zhang, M.; Zhang, Y.; Lyu, J.; Yang, H. The effect of the secondary air injection on the gas–solid flow characteristics in the circulating fluidized bed. *Chem. Eng. Res. Des.* **2019**, *141*, 220–228. [CrossRef]
26. Jordan, C.A.; Akay, G. Speciation and distribution of alkali, alkali earth metals and major ash forming elements during gasification of fuel cane bagasse. *Fuel* **2012**, *91*, 253–263. [CrossRef]
27. Zevenhoven-Onderwater, M.; Backman, R.; Skrifvars, B.J.; Hupa, M. The ash chemistry in fluidised bed gasification of biomass fuels. Part I: Predicting the chemistry of melting ashes and ash–bed material interaction. *Fuel* **2001**, *80*, 1489–1502. [CrossRef]
28. Pettersson, A.; Åmand, L.E.; Steenari, B.M. Chemical fractionation for the characterisation of fly ashes from co-combustion of biofuels using different methods for alkali reduction. *Fuel* **2009**, *88*, 1758–1772. [CrossRef]
29. Zhao, Y.; Feng, D.; Zhang, Y.; Huang, Y.; Sun, S. Effect of pyrolysis temperature on char structure and chemical speciation of alkali and alkaline earth metallic species in biochar. *Fuel Process. Technol.* **2016**, *141*, 54–60. [CrossRef]
30. Feng, D.D.; Guo, D.W.; Zhang, Y.; Sun, S.Z.; Zhao, Y.J.; Chang, G.Z.; Guo, Q.J.; Qin, Y.K. Adsorption-enrichment characterization of CO_2 and dynamic retention of free NH_3 in functionalized biochar with H_2O/NH_3 center dot H2O activation for promotion of new ammonia-based carbon capture. *Chem. Eng. J.* **2021**, *409*, 128193. [CrossRef]
31. Feng, D.D.; Zhao, Y.J.; Zhang, Y.; Sun, S.Z.; Gao, J.M. Steam Gasification of Sawdust Biochar Influenced by Chemical Speciation of Alkali and Alkaline Earth Metallic Species. *Energies* **2018**, *11*, 205. [CrossRef]
32. Wang, W.; Wang, Q.; Lyu, J.; Liu, M.; Yue, G.; Liu, J. The Effect of Inner Secondary Air on the Flow Field of a Swirl Burner. In Proceedings of the 2nd International Conference on Smart Power & Internet Energy Systems (SPIES), Bangkok, Thailand, 15–18 September 2020; pp. 452–456.
33. Lv, J.; Li, D. Effect of temperature on the characteristics of primary particles in pulverized coal combustion. *Chin. J. Electr. Eng.* **2007**, *27*, 24–29.
34. Nguyen, C.B.; Scherer, J.; Hartwich, M.; Richter, A. The morphology evolution of char particles during conversion processes. *Combust. Flame* **2021**, *226*, 117–128. [CrossRef]
35. Yaroshchuk, A. Evaporation-driven electrokinetic energy conversion: Critical review, parametric analysis and perspectives. *Adv. Colloid Interface Sci.* **2022**, *305*, 102708. [CrossRef]
36. Hao, Z.; Xie, G.; Liu, X.; Tan, Q.; Wang, R. The precipitation behaviours and strengthening mechanism of a Cu-0.4 wt% Sc alloy. *J. Mater. Sci. Technol.* **2022**, *98*, 1–13. [CrossRef]

37. Lu, Y.; Cao, R.; Huang, D.W.; Cui, Z.N.; Wang, Y.; Zhang, Y.F. Investigation on the ash characteristics and AAEM migration during co-combustion of Zhundong coal and shale char in a fixed bed. *Fuel* **2022**, *327*, 125214. [CrossRef]
38. Lighty, J.S.; Veranth, J.M.; Sarofim, A.F. Combustion aerosols: Factors governing their size and composition and implications to human health. *J. Air Waste Manag. Assoc.* **2000**, *50*, 1619–1622. [CrossRef]
39. Zhang, L.; Ninomiya, Y.; Yamashita, T. Formation of submicron particulate matter (PM 1) during coal combustion and influence of reaction temperature. *Fuel* **2006**, *85*, 1446–1457. [CrossRef]
40. Wood, B.J.; Smythe, D.J.; Harrison, T. The condensation temperatures of the elements: A reappraisal. *Am. Mineral. J. Earth Planet. Mater.* **2019**, *104*, 844–856. [CrossRef]
41. Wang, Y.B.; Tan, H.Z. Condensation of KCl(g) under varied temperature gradient. *Fuel* **2019**, *237*, 1141–1150. [CrossRef]
42. Zhang, Y.; Shang, Q.; Feng, D.D.; Sun, H.L.; Wang, F.H.; Hu, Z.C.; Cheng, Z.Y.; Zhou, Z.J.; Zhao, Y.J.; Sun, S.Z. Interaction mechanism of in-situ catalytic coal H_2O-gasification over biochar catalysts for H_2O-H_2-tar reforming and active sites conversion. *Fuel Process. Technol.* **2022**, *233*, 107307. [CrossRef]
43. Feng, D.D.; Zhang, Y.; Zhao, Y.J.; Sun, S.Z.; Wu, J.Q.; Tan, H.P. Mechanism of in-situ dynamic catalysis and selective deactivation of H2O-activated biochar for biomass tar reforming. *Fuel* **2020**, *279*, 118450. [CrossRef]
44. Hu, Y.; Lu, H.; Liu, W.; Yang, Y.; Li, H. Incorporation of CaO into inert supports for enhanced CO_2 capture: A review. *Chem. Eng. J.* **2020**, *396*, 125253. [CrossRef]
45. Pi, S.; Zhang, Z.; He, D.; Qin, C.; Ran, J. Investigation of Y_2O_3/MgO-modified extrusion–spheronized CaO-based pellets for high-temperature CO_2 capture. *Asia-Pac. J. Chem. Eng.* **2019**, *14*, e2366. [CrossRef]
46. Zhang, Y.; Wang, S.Z.; Feng, D.D.; Gao, J.M.; Dong, L.H.; Zhao, Y.J.; Sun, S.Z.; Huang, Y.D.; Qin, Y.K. Functional Biochar Synergistic Solid/Liquid-Phase CO_2 Capture: A Review. *Energy Fuels* **2022**, *36*, 2945–2970. [CrossRef]
47. Feng, D.D.; Zhao, Y.J.; Zhang, Y.; Xu, H.H.; Zhang, L.Y.; Sun, S.Z. Catalytic mechanism of ion-exchanging alkali and alkaline earth metallic species on biochar reactivity during CO_2/H_2O gasification. *Fuel* **2018**, *212*, 523–532. [CrossRef]
48. Jiang, S.; Xu, H.; Sun, Y.; Song, Y. Performance analysis of Fe-N compounds based on valence electron structure. *J. Alloys Compd.* **2019**, *779*, 427–432. [CrossRef]
49. Helble, J.J. Mechanisms of Ash Formation and Growth During Pulverized Coal Combustion. Ph.D. Thesis, Department of Chemical Engineering, Massachusetts Institute of Technology, Cambridge, MA, USA, 1987.